

Chapter 2

Thin Disc Embedded in Extended Spherically Symmetric Cluster

In Sect. 1.7, we have investigated the orbital evolution of thin isolated stellar discs around the SMBH. There is statistically significant evidence that such structures, indeed, are present in galactic nuclei (Levin and Beloborodov 2003; Bender et al. 2005; Paumard et al. 2006; Bartko et al. 2009, 2010; Lauer et al. 2012). In this case, however, it is reasonable to expect the stellar disc to be embedded in an extended spherically symmetric relaxed star cluster that is centred on the SMBH. Hence, in this chapter, we focus on how the orbital evolution of the stellar discs is affected if we include the spherical perturbation.

2.1 The Cluster Modelled by Analytic Potential

In the first step, we emulate the gravity of the extended spherical star cluster by an analytic spherically symmetric potential, i.e. we neglect the fluctuating component of the total potential generated by the cluster. In order to test whether such a perturbation has an impact upon the relaxation of the disc, we consider the same stellar disc as in Sect. 1.7 and include the potential that corresponds to the spherically symmetric mass distribution described by the Bahcall-Wolf radial density profile (1.30) (see model B1 in Table 2.1 for the particular values of the model parameters). As this profile is expected to describe the structure of relaxed spherical star clusters that contain a massive central body (see Sect. 1.6), it represents a natural choice for modelling the mean potential of the cluster in our calculations. The strength of the potential is characterized by the mass, $M_c(R_{\text{out}})$, of the cluster enclosed within the outer radius of the disc, $R_{\text{out}} = 10 R_{\text{in}}$, and we set $M_c(R_{\text{out}}) = 0.01 M_\bullet$.

Figure 2.1 shows the evolution of the root-mean-square eccentricity, e_{rms} , and inclination, i_{rms} , of the orbits in the disc (solid lines). If we compare the results with those acquired for the isolated stellar disc (dashed lines; redrawn from Fig. 1.7; model B0), we cannot identify any significant difference, except for the initially larger values of e_{rms} due to the effectively larger mass enclosed within the orbits. Similar results can be obtained even for larger characteristic masses $M_c(R_{\text{out}})$, as long as the

Table 2.1 Parameters of the numerical models described in Chaps. 1 and 2

	B0	B1	canon.	H	M	A	D
N -body disc	yes	yes	yes	yes	yes	yes	yes
N -body cluster	–	–	yes	yes	yes	yes	yes
Predef. cluster	–	yes	–	–	yes	–	–
Predef. ring	–	–	–	–	–	–	–
N_{d1}	600	600	600	600	600	600	600
m_{d1} [$10^{-6} M_{\bullet}$]	2.5	2.5	2.5	2.5	2.5	2.5	2.5
N_{d2}	300	300	300	300	300	300	300
m_{d2} [$10^{-6} M_{\bullet}$]	7.5	7.5	7.5	7.5	7.5	7.5	7.5
N_{d3}	100	100	100	100	100	100	100
m_{d3} [$10^{-6} M_{\bullet}$]	25	25	25	25	25	25	25
$a_{d,\min}-a_{d,\max}$ [R_{in}]	1–10	1–10	1–10	1–10	1–10	1–10	1–10
α_d	–1	–1	–1	–1	–1	–1	–1
e_d	gc	gc	gc	gc	gc	gc	gc
Δ [$^{\circ}$]	2.5	2.5	2.5	2.5	2.5	2.5	2.5
N_c [10^3]	–	–	12.5	100	6.25	50	6.25
m_c [$10^{-6} M_{\bullet}$]	–	–	1.903	2.378	3.806	0.476	3.806
$a_{c,\min}-a_{c,\max}$ [R_{in}]	–	–	0.5–20	0.5–20	0.5–20	0.5–20	0.5–20
α_c	–	–	1/4	1/4	1/4	1/4	1/4
e_c	–	–	gc	gc	gc	gc	gc
$M_c(R_{out})$ [$10^{-2} M_{\bullet}$]	–	1	–	–	1	–	–
β_c	–	–7/4	–	–	–7/4	–	–
M_r [$10^{-1} M_{\bullet}$]	–	–	–	–	–	–	–
R_r [R_{in}]	–	–	–	–	–	–	–
i_r	–	–	–	–	–	–	–
Num. integrator	N	N	N	N	N	N	N
				K0a	K0b	K1a	K1b
N -body disc				–	–	yes	yes
N -body cluster				yes	yes	–	–
Predef. cluster				–	–	–	–
Predef. ring				yes	yes	yes	yes
N_{d1}				–	–	300	300
m_{d1} [$10^{-6} M_{\bullet}$]				–	–	tp	4
N_{d2}				–	–	–	–
m_{d2} [$10^{-6} M_{\bullet}$]				–	–	–	–
N_{d3}				–	–	–	–
m_{d3} [$10^{-6} M_{\bullet}$]				–	–	–	–
$a_{d,\min}-a_{d,\max}$ [R_{in}]				–	–	1–1.8	1–1.8
α_d				–	–	–1	–1
e_d				–	–	0–0.1	0–0.1
Δ [$^{\circ}$]				–	–	2.5	2.5

(continued)

Table 2.1 (continued)

	K0a	K0b	K1a	K1b
$N_c [10^3]$	0.6	0.6	–	–
$m_c [10^{-6} M_\bullet]$	tp	25	–	–
$a_{c,\min}-a_{c,\max} [R_{\text{in}}]$	1–3*	1–3*	–	–
α_c	1/4	1/4	–	–
e_c	0–0.1	0–0.1	–	–
$M_c(R_{\text{out}}) [10^{-2} M_\bullet]$	–	–	–	–
β_c	–	–	–	–
$M_r [10^{-1} M_\bullet]$	1	1	0.5	0.5
$R_r [R_{\text{in}}]$	12*	12*	6	6
i_r	–	–	$\pi/2$	$\pi/2$
Num. integrator	M	M	M	M

The first five rows give the model designation and included components in order: the N -body disc, the N -body cluster, the predefined analytic cluster and the predefined analytic ring. The subsequent rows describe the initial properties of the N -body disc: numbers (N_{d1} , N_{d2} , N_{d3}) and masses (m_{d1} , m_{d2} , m_{d3}) of the particles in the disc, interval ($a_{d,\min}$, $a_{d,\max}$) and power-law index (α_d) of the initial distribution of the orbital semi-major axes in the disc, initial eccentricities of the orbits in the disc (e_d) and initial half-opening angle of the disc (Δ). The analogical quantities indexed by ‘c’ describe the initial properties of the N -body cluster. The characteristic mass of the predefined analytic cluster within the initial outer radius of the disc R_{out} and the power-law index of the corresponding radial density profile, $\rho \sim r^{\beta_c}$, are denoted $M_c(R_{\text{out}})$ and β_c , respectively. The predefined analytic ring is described by its mass M_r , radius R_r and inclination i_r with respect to the plane of the disc. The row ‘Num. integrator’ indicates which N -body integration code has been used for the particular model: NBODY6 (N; Aarseth 2003) and Mbody (M; Šubr 2006). The abbreviation ‘gc’ indicates that the orbits are constructed to be geometrically circular; ‘tp’ stands for ‘test particles’ with extremely low mass $2.5 \times 10^{-12} M_\bullet$. In the case of models K0a and K0b, the length unit is chosen to be the inner radius of the cluster since these models do not include any disc whose inner radius, R_{in} , represents the length unit in the remaining models (the affected values are marked by an asterisk)

potential of the cluster may be considered a perturbation to the dominating potential of the SMBH ($M_c(R_{\text{out}}) \lesssim 0.1 M_\bullet$). In conclusion, we find that the gravitational perturbation in the form of an analytic spherically symmetric potential does not affect relaxation of the angular momentum in the disc.

Furthermore, comparison of the evolved distributions of the orbital semi-major axes displayed in Fig. 2.2 reveals that, within both models, the distributions are of the same shape. Hence, it appears that neither the energy transfer in the disc is affected if the analytic spherical cluster is included. The case when the cluster is modelled by a large number of gravitating, mutually interacting particles is described in the following section.

2.2 Coupling of the Disc and the Cluster

In order to investigate the orbital evolution of the thin stellar disc under the gravitational influence of the spherical cluster which is treated in the full N -body way, we introduce the following configuration:

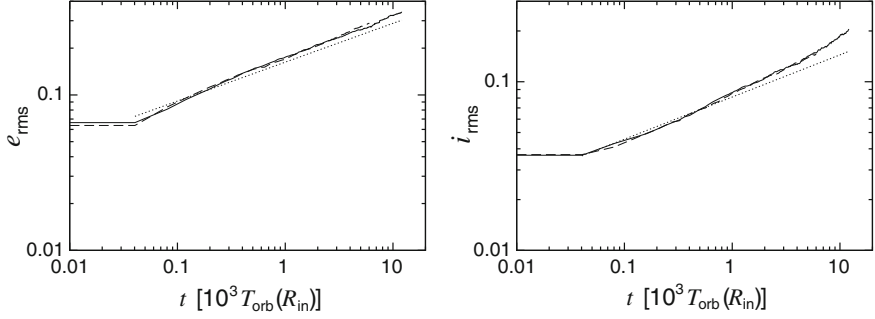


Fig. 2.1 Evolution of the root-mean-square eccentricity e_{rms} (left panel) and inclination i_{rms} (right panel) of the orbits in the stellar disc around the SMBH in a predefined analytic spherically symmetric potential (solid lines; model B1) in comparison to the previously discussed case of the isolated stellar disc (dashed lines; redrawn from Fig. 1.7; model B0). Time is given in multiples of the orbital period that corresponds to the initial inner radius of the orbits in the disc, R_{in} . The thin-dotted lines denote the theoretical $t^{1/4}$ dependence derived for the isolated stellar discs (see Eqs. (1.45) and (1.46)). The displayed results correspond to 1 realization of the models. In the case of model B1, the parameters are the same as in Fig. 1.7, except for $M_{\text{c}}(R_{\text{out}}) = 0.01 M_{\bullet}$ (see also Table 2.1)

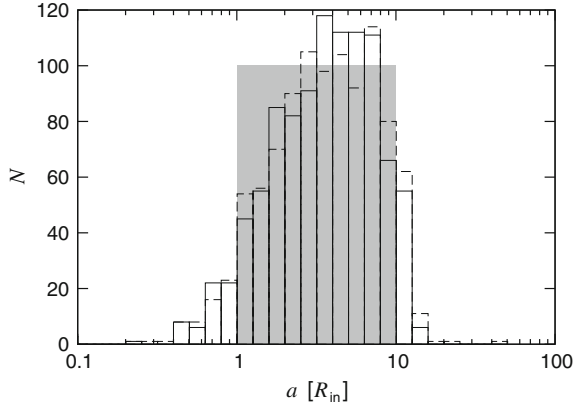


Fig. 2.2 Evolution of the distribution of the orbital semi-major axes in the stellar disc around the SMBH in a predefined analytic spherically symmetric potential (solid boxes; model B1) in comparison to the previously discussed case of the isolated stellar disc (dashed boxes; redrawn from Fig. 1.8; model B0). The initial distribution (grey rectangle) is the same in both cases. The evolved distributions describe the state at $t \approx 10^4 T_{\text{orb}}(R_{\text{in}})$. The displayed results correspond to 1 realization of the models. In the case of model B1, the parameters are the same as in Fig. 1.8, except for $M_{\text{c}}(R_{\text{out}}) = 0.01 M_{\bullet}$ (see also Table 2.1)

- the SMBH of mass M_{\bullet} is considered to be a fixed source of static Keplerian potential, $\phi_{\bullet}(r) = -GM_{\bullet}/r$,
- the stellar disc is modelled as a group of N_{d} interacting stars of mass m_{d} ; the semi-major axes of the stellar orbits in the disc are initially distributed according to $dN/da \propto a^{\alpha_{\text{d}}}$, $a \in \langle a_{\text{d,min}}, a_{\text{d,max}} \rangle$; the disc is considered to be initially thin with half-opening angle Δ ,

- the spherical star cluster is treated as N_c interacting stars of mass m_c ; initial distribution of the semi-major axes of the orbits in the cluster obeys $dN/da \propto a^{\alpha_c}$, $a \in \langle a_{c,\min}, a_{c,\max} \rangle$.

Temporal evolution of this stellar system is followed numerically, by means of the N -body integration code NBODY6 (Aarseth 2003). The Keplerian potential of the SMBH has been incorporated into the publicly available version of the code as an additional external potential. The original code has also been optimized for integrations of the massive central body dominated stellar systems in cooperation with its author, Sverre J. Aarseth. The xy -plane of our Cartesian reference frame is defined by the plane of symmetry of the disc. The stellar motions in the disc are considered to be initially prograde, i.e. the reference z -axis is pointing to the same hemisphere as the initial mean angular momentum of the disc.

We start with a particular setup (hereafter ‘canonical’ configuration; see also Table 2.1) that is primarily motivated by the stellar system observed in the Galactic Centre and discuss the acquired results later on (see Sect. 2.4). For simplicity, the stellar orbits in both the cluster and the disc are constructed to be initially geometrically circular. Although this setup is not very realistic for the orbits in the cluster, it can still provide useful insights into the evolution of general non-circular stellar systems.

The parameters of the disc are the same as in the previous section. In particular, the individual stars are assumed to have one of the following three masses: $m_{d1} = 2.5 \times 10^{-6} M_\bullet$, $m_{d2} = 7.5 \times 10^{-6} M_\bullet$, $m_{d3} = 2.5 \times 10^{-5} M_\bullet$. The corresponding abundances are $N_{d1} = 600$, $N_{d2} = 300$ and $N_{d3} = 100$, yielding the total mass of the disc $N_{d1}m_{d1} + N_{d2}m_{d2} + N_{d3}m_{d3} = 6.25 \times 10^{-3} M_\bullet$. The initial distribution of the orbital elements is independent of the stellar mass. The power-law index for the initial distribution of the radii, R , of the orbits in the disc is set to $\alpha_d = -1$. This value corresponds to the surface density profile, $\Sigma(R) \propto R^{-2}$, that has been recently reported to describe the stellar disc observed in the innermost parsec of our Galaxy (Paumard et al. 2006, see also Chap. 4 of this thesis for details). The initial interval for the radii of the orbits spreads over one order of magnitude, $R \in \langle R_{\text{in}}, 10R_{\text{in}} \rangle$, where R_{in} denotes the initial inner radius of the disc. The disc is considered to have the initial half-opening angle $\Delta = 2.5^\circ$. The initial distributions of the orbital nodal longitudes, Ω , and arguments of pericentre, ω , are uniform, in accord with the assumption that the disc is initially axially symmetric.

The cluster consists, in the canonical configuration, of $N_c = 1.25 \times 10^4$ equal-mass stars with $m_c \approx 1.9 \times 10^{-6} M_\bullet$. The total mass of the cluster thus is $N_cm_c \approx 0.02 M_\bullet$. The initial distribution of the radii of the orbits in the cluster, $R \in \langle 0.5 R_{\text{in}}, 20 R_{\text{in}} \rangle$, obeys the power-law with index $\alpha_c = 1/4$ which corresponds to the Bahcall-Wolf radial density profile (1.30). Hence, the mass of the cluster enclosed within the initial outer radius of the disc, R_{out} , equals the characteristic mass $M_c(R_{\text{out}}) = 0.01 M_\bullet$ considered in the previous section. Since we assume the cluster to be initially spherically symmetric, the distributions of $\cos i$, Ω and ω of the orbits in the cluster are initially uniform.

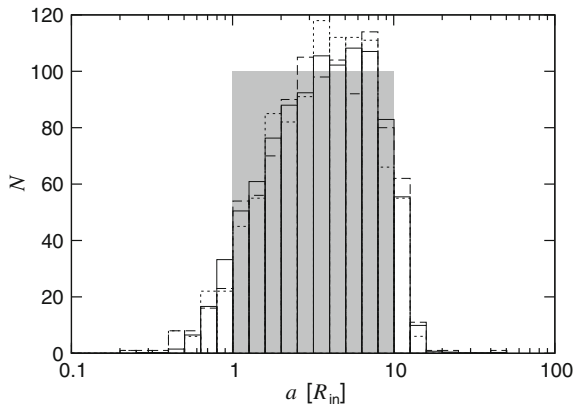


Fig. 2.3 Evolution of the orbital semi-major axes in the disc embedded in the spherical cluster in terms of their initial distribution (*grey rectangle*) and its evolved state at $t \approx 10^4 T_{\text{orb}}(R_{\text{in}})$ for three different treatments of the cluster gravity: no cluster included (*dashed boxes*; see also Sect. 1.7 and Table 2.1, model B0), predefined analytic potential (*dotted boxes*; see also Sect. 2.1 and Table 2.1, model B1) and the cluster treated as a large number of gravitating stars (*solid boxes*; canonical configuration, see Table 2.1). We see that the evolved states are roughly the same in all three cases. The displayed results for the canonical configuration are averaged over 9 realizations. In the remaining two cases, the distributions describe 1 realization

2.2.1 Accelerated Exchange of Angular Momentum

Our calculations show (see also Haas and Šubr 2012) that the full N -body treatment of the cluster gravity does not affect the evolution of the distribution of the orbital semi-major axes in the disc in any noticeable way. Figure 2.3 demonstrates this finding. It shows the comparison of the initial distribution (grey rectangle) and its state at $t \approx 10^4 T_{\text{orb}}(R_{\text{in}})$ in three different cases. The previously discussed results for the models with no cluster included and the cluster represented by an analytic potential are depicted by the dashed and dotted boxes, respectively (see Sects. 1.7 and 2.1 for details). The newly introduced canonical model with the full N -body treatment of the cluster gravity is denoted by the solid boxes. As we can see, the evolved distributions are similar in all three cases, which indicates that the energy transfer in the disc is dominated by its high stellar density rather than by the gravitational interaction with the embedding cluster.

On the other hand, we find that the full N -body treatment of the cluster gravity has a significant impact upon the exchange of angular momentum. Figure 2.4 shows the evolution of the root-mean-square eccentricity, e_{rms} , (left panel) and inclination, i_{rms} , (right panel) of the stellar orbits in the disc. We see that, although the initial phase is nearly identical in all three cases, at some moment, evolution of both elements is accelerated if the cluster is treated as a group of gravitating stars (solid lines). Our results, discussed in detail below, show that this acceleration is due to averaging over an increasing number of orbits whose eccentricity and inclination start to oscillate to

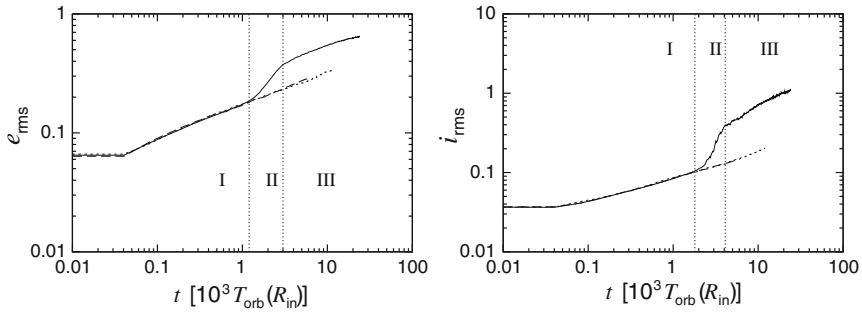


Fig. 2.4 Evolution of the root-mean-square eccentricity e_{rms} (left panel) and inclination i_{rms} (right panel) of the stellar orbits in the disc embedded in the spherical cluster for the same three treatments of the cluster gravity as in Fig. 2.3. Time is given in multiples of the orbital period that corresponds to the initial inner radius of the orbits in the disc, R_{in} . We see that in the case of the cluster modelled in the full N -body way (solid lines; canonical configuration), the evolution of both elements is accelerated. The displayed results for the canonical configuration are averaged over 9 realizations. In the remaining two cases, the curves describe 1 realization (model parameters are summarized in Table 2.1)

very high values. We further suggest that these oscillations are caused by the Kozai-Lidov dynamics in the combined potential of the disc and a system of flattened structures that, according to our computations, form in the cluster.

2.2.2 e -Instability in the Cluster

As we have already mentioned above, the initially spherically symmetric cluster develops macroscopic non-spherical structures. It turns out that this is due to the gravity of the embedded thin disc. In this section, we describe the formation of these structures whose gravitational potential, subsequently, influences the orbits of the stars from the disc.

In the initial phase of the evolution of the cluster (i.e. before the non-spherical structures are formed), the individual stellar orbits in the cluster can be, in principle, affected by the following processes:

- the Kozai-Lidov mechanism in the axisymmetric potential of the disc,
- negative pericentre shift due to the spherical mean potential of the cluster,
- two-body and resonant relaxation of the cluster.

In order to determine which of these processes are effective enough to have an impact on the initial phase of the cluster evolution in the canonical configuration, we evaluate their characteristic timescales for this particular setting. For this purpose, we first focus on the inner parts of the cluster where, according to our results, the formation of the macroscopic non-spherical perturbation begins. The evolution of the outer parts of the cluster is described in Sect. 2.2.6.

The characteristic Kozai-Lidov time-scale (1.13) in the case of a disc-like perturber reads $T_{\text{KL}} \sim (M_{\bullet}/M_{\text{d}})(R_{\text{d}}/R)^3 T_{\text{orb}}$, where M_{d} and R_{d} are the mass and characteristic radius of the disc, respectively, R is the radius of the orbit and $T_{\text{orb}} \sim \sqrt{R^3/GM_{\bullet}}$. For the canonical radial density profile of the disc, we estimate $R_{\text{d}} \sim R_{\text{in}}$. Since $R \sim R_{\text{in}}$ in the inner parts of the cluster, the ratio R_{d}/R is of order unity. In the canonical configuration, the mass of the disc, $M_{\text{d}} = N_{\text{d1}}m_{\text{d1}} + N_{\text{d2}}m_{\text{d2}} + N_{\text{d3}}m_{\text{d3}}$, is of order $\sim 10^{-3} M_{\bullet}$ and, therefore, $T_{\text{KL}} \sim 10^3 T_{\text{orb}}$. The timescale for the pericentre shift (1.22) can be written as $T_{\text{c}} \sim (M_{\bullet}/N_{\text{c}}(R)m_{\text{c}}) T_{\text{orb}}$, where $N_{\text{c}}(R)$ is the number of the stars in the cluster enclosed within radius R . For $R \sim R_{\text{in}}$, we have $N_{\text{c}}(R_{\text{in}}) \sim 10^2$. Hence, considering the mass of the stars in the cluster $m_{\text{c}} \sim 10^{-6} M_{\bullet}$, we obtain $T_{\text{c}} \sim 10^4 T_{\text{orb}}$. The characteristic timescale for the vector resonant relaxation in the cluster (1.33) can be, in the canonical configuration, expressed as $T_{\text{vr,sf}} \sim (M_{\bullet}/N_{\text{c}}(R)^{1/2} m_{\text{c}}) T_{\text{orb}}$. For $R \sim R_{\text{in}}$, we have $N_{\text{c}}(R_{\text{in}})^{1/2} \sim 10$ and $T_{\text{vr,sf}} \sim 10^5 T_{\text{orb}}$. The characteristic timescales of the scalar resonant relaxation and the two-body relaxation of the cluster are even longer (see Sect. 1.6).

The initial phase of the orbital evolution of the cluster covers a period of time of order $\sim 10^3 T_{\text{orb}}(R_{\text{in}})$, as can be inferred, e.g. from Fig. 2.6 which we describe below. Hence, neither two-body nor resonant relaxation of the cluster can significantly affect the individual stellar orbits from its inner parts during this phase of the evolution. On the other hand, the Kozai-Lidov mechanism in the axisymmetric potential of the disc is efficient enough to have an impact on these orbits. Furthermore, since $T_{\text{c}} \sim 10^4 T_{\text{orb}}(R_{\text{in}})$, we cannot safely exclude the effect of the pericentre shift in the mean potential of the cluster. In fact, our calculations show that for most of the orbits in the cluster with the initial radius $> R_{\text{in}}$, the Kozai-Lidov oscillations are damped by the mean spherical potential of the cluster during the initial phase of their evolution. This is demonstrated in Fig. 2.5 which displays the evolution of the orbital elements for a typical star from the innermost parts of the cluster (initial radius of the orbit $\approx R_{\text{in}}$). As we can see, both eccentricity e (dashed line) and inclination i (solid line) remain roughly constant until $t \approx 2 \times 10^3 T_{\text{orb}}(R_{\text{in}})$. The nodal longitude Ω (dotted line) and argument of pericentre ω (dot-dashed line) of the orbit show a secular rotation. In the case of the nodal longitude, the rotation is, for this particular star, rather slow due to the high inclination of the stellar orbit since $d\Omega/dt \propto \cos i \rightarrow 0$ for $i \rightarrow \pi/2$ (see Eqs. (1.12)). In conclusion, we find that, in the initial phase of the evolution of the cluster, the stellar orbits from its inner parts undergo combined precession of their nodal and apsidal lines only, keeping their eccentricity and inclination close to their initial values.

Our results further show that the orbits from the inner parts of the cluster tend to change their orientations in a way such that their eccentricity vectors, \mathbf{e} , are pointing in similar directions, parallel to the plane of the disc. Figure 2.6 illustrates this finding by means of sinusoidal projection of eccentricity vectors of the stars from the cluster whose osculating semi-major axis, a , fulfils $a < 1.5 R_{\text{in}}$. In the initial state (top-left panel), the orbits are distributed uniformly over the whole plot, which is in accord with the assumed initial spherical symmetry of the cluster. In the other panels, however, we observe that most of the orbits tend to form a rather compact

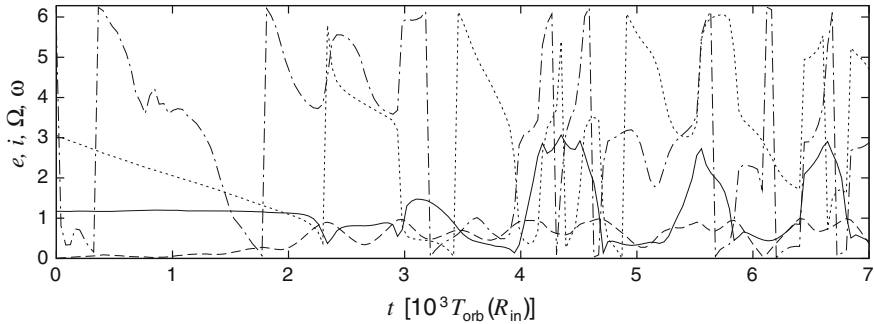


Fig. 2.5 Evolution of the orbital eccentricity e (dashed line), inclination i (solid line), nodal longitude Ω (dotted line) and argument of pericentre ω (dot-dashed line) of a typical stellar orbit from the innermost parts of the cluster in the canonical configuration (parameters summarized in Table 2.1). We see that, in the initial phase of the evolution, the Kozai-Lidov oscillations are damped by the mean spherical potential of the cluster ($t \lesssim 2 \times 10^3 T_{\text{orb}}(R_{\text{in}})$). When the e -structure in the cluster is formed, the orbit undergoes its Kozai-Lidov cycles ($2 \times 10^3 T_{\text{orb}}(R_{\text{in}}) \lesssim t \lesssim 3.5 \times 10^3 T_{\text{orb}}(R_{\text{in}})$). Subsequently, it is captured by the e -structure in the disc, thus showing typical oscillations of eccentricity and inclination ($t \gtrsim 3.5 \times 10^3 T_{\text{orb}}(R_{\text{in}})$)

group which is located on the equatorial line ($i_e = 90^\circ$) of the plots. Hereafter, we refer to this type of orbital structure, as the e -structure. We point out that, despite the similar orientations of the eccentricity vectors of the individual orbits in the e -structure, the initial spherical symmetry of the mass distribution in the cluster is disturbed only slightly. Nevertheless, our results indicate that the small deviation from the initial symmetry is sufficient for the e -structure to have a significant impact upon the evolution of the disc. Let us also note that the two horizontal features visible in the top-right and bottom-left panels of Fig. 2.6 are only temporary and we explain their origin in Sect. 2.3.1.

Although the process of formation of the e -structure is not fully clear yet, we suggest that it can be understood in the following way. As mentioned above, the orbits from the cluster undergo combined nodal and apsidal precession. Since the rate of this precession depends on the orbital elements, individual orbits precess at different rates, which leads to a change of their relative orientations. Consequently, also the strength of the long-term mutual interaction of the stars on these orbits is changed. We suggest that, once two (or more) orbits achieve a specific orientation in which their mutual interaction is strong enough, they tend to dynamically couple together and precess further synchronously. Furthermore, once the orbits become dynamically coupled, the probability of capture of another orbit increases as the potential well of multiple coupled orbits is deeper than those of the individual orbits. As a result, coupling of the individual orbits turns into e -instability and the initially spherically symmetric cluster gradually forms a single e -structure that includes most of the stars from the affected region.

According to our calculations, the e -structure slowly rotates around the symmetry axis of the disc on a timescale of the order of magnitude $\sim 10 T_{\text{KL}}(R_{\text{in}})$. Although the

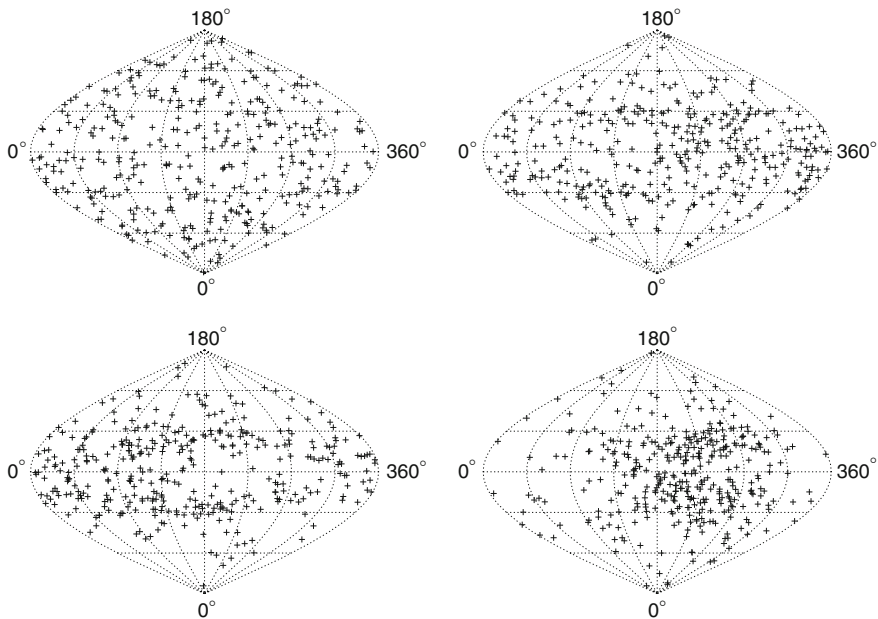


Fig. 2.6 Directions of the eccentricity vectors of the individual stars from the cluster with the osculating semi-major axes $a < 1.5 R_{\text{in}}$ in terms of angles Ω_e (abscissa) and i_e (ordinate) in sinusoidal projection. The plots describe the state at four different times: $t = 0$ (*top-left panel*), $t \approx 0.6 \times 10^3 T_{\text{orb}}(R_{\text{in}})$ (*top-right panel*), $t \approx 1.2 \times 10^3 T_{\text{orb}}(R_{\text{in}})$ (*bottom-left panel*), and $t \approx 1.8 \times 10^3 T_{\text{orb}}(R_{\text{in}})$ (*bottom-right panel*). The initial state corresponds to the initial spherical symmetry of the cluster. Subsequently, we observe formation of the e -structure (the compact group in the plots). The two horizontal features in the in the *top-right* and *bottom-left panel* are temporary (see Sect. 2.3.1). Model parameters are set to their canonical values (see Table 2.1)

rate of rotation of the individual orbits strongly fluctuates around the mean rotation of the e -structure as a whole, these fluctuations are not strong enough to disrupt the ongoing formation of the e -structure. The direction in which the e -structure rotates depends on the mean inclination, $\langle i \rangle$, of the orbits in the e -structure. In particular, we find that the rotation is opposite for $\langle i \rangle < \pi/2$ and $\langle i \rangle > \pi/2$. Furthermore, our results show that the eccentricities and inclinations of the orbits near the outer edge of the e -structure are similar to the initial conditions for the cluster, i.e. these orbits are rather low-eccentric and the distribution of their $\cos i$ is roughly uniform, yielding the mean inclination of $\approx \pi/2$ (see the crosses in the right panel of Fig. 2.7). On the other hand, the orbits with smaller semi-major axes (circles in the right panel of Fig. 2.7) have higher eccentricities. We suggest that this can be explained by the following argument.

As we have already mentioned, the spherically symmetric mean potential of the cluster suppresses, until the e -structure is formed, the Kozai-Lidov mechanism in the potential of the disc. Hence, the individual orbits from the cluster retain their eccentricity and inclination close to their initial values. Upon the formation of the

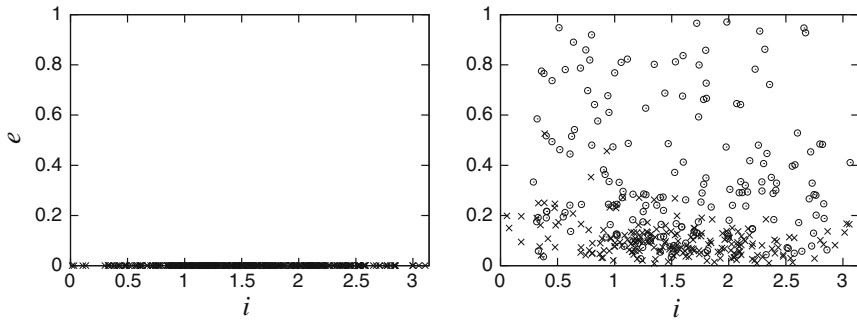


Fig. 2.7 Eccentricity e and inclination i of the orbits from the innermost parts of the cluster: orbits with the osculating semi-major axis $a < R_{\text{in}}$ and $R_{\text{in}} < a < 1.5 R_{\text{in}}$ are denoted by *circles* and *crosses*, respectively. The initial state is shown in the *left panel*. The *right panel* describes the state at $t \approx 1.2 \times 10^3 T_{\text{orb}}(R_{\text{in}})$. We see that the orbits with larger osculating semi-major axes (*crosses*) are still low-eccentric even when a significant e -structure is formed (cf. the *bottom-left panel* of Fig. 2.6). On the other hand, the orbits with smaller semi-major axes are already oscillating (*circles*). Model parameters are set to their canonical values (see Table 2.1)

e -structure, however, the spherical symmetry of the mean potential is disturbed and, therefore, its damping effect is weaker. Consequently, the Kozai-Lidov mechanism in the potential of the disc starts to affect the orbits in the e -structure which thus undergo the high-amplitude Kozai-Lidov oscillations of eccentricity and inclination. As the Kozai-Lidov timescale (1.13) depends strongly upon the semi-major axis and, furthermore, since the e -instability gradually propagates from the centre of the cluster outwards (see Sect. 2.2.6 for details), the orbits in the central parts of the e -structure are already oscillating while the elements of the orbits near its outer edge are still unaffected.

The onset of the Kozai-Lidov mechanism in the potential of the disc after the formation of the e -structure is also visible in Fig. 2.5. In particular, we see that all of the displayed orbital elements evolve, in the interval $2 \times 10^3 T_{\text{orb}}(R_{\text{in}}) \lesssim t \lesssim 3.5 \times 10^3 T_{\text{orb}}(R_{\text{in}})$, in a way that corresponds to the lower librational lobe (around $\omega = 3\pi/2$) in the Kozai-Lidov diagrams (see Sect. 1.3, Figs. 1.2 and 1.3).

In the context of these findings, we argue that the e -structure represents, shortly after its formation, a flattened stellar overdensity which is roughly perpendicular to the plane of the disc. Moreover, due to the fact that the frequencies of the nodal and apsidal precessions in the Kozai-Lidov mechanism are similar, the orbits from the e -structure that subsequently undergo their Kozai-Lidov cycles roughly preserve the orientation of their apsidal lines (the small deviations are ‘absorbed’ by the other orbits due to their mutual interaction). Consequently, the coherent rotation of the e -structure is not disturbed and, therefore, the Kozai-Lidov oscillations of eccentricity and inclination of the orbits in the e -structure do not disturb its overall shape. The orbits are either highly inclined and low-eccentric or they are found in the plane of the disc but have very high eccentricities. As a result, the slowly rotating e -structure remains flattened and its potential causes, in return, the Kozai-Lidov mechanism in the disc.

2.2.3 Orbital Evolution of the Disc

Now, that we have briefly outlined the orbital evolution of the cluster, we have sufficient information to explain the accelerated increase of the root-mean-square eccentricity and inclination of the stellar orbits from the disc observed in Fig. 2.4. During the initial phase of the evolution (denoted as ‘I’), the mean potential of the cluster is spherically symmetric and, as such, has no impact upon the evolution of the orbital eccentricities and inclinations in the disc. Furthermore, the evolution of eccentricity and inclination is not affected by the relaxation in the fluctuating potential of the cluster as this process operates on timescales that are by two orders of magnitude longer than the initial phase of the evolution itself. Hence, during this phase, the disc evolves solely due to its two-body relaxation whose characteristic timescale (1.36) is very short since the orbits in the disc are initially nearly circular. The evolution of the root-mean-square eccentricity and inclination of the orbits from the disc is thus similar to the evolution found in the cases with the cluster emulated by the predefined analytic potential and with no cluster present at all.

When the e -structure in the cluster is formed, however, its potential starts to induce the Kozai-Lidov oscillations with combined nodal and apsidal precession of the orbits in the disc with respect to the plane of the e -structure. Since this plane is roughly perpendicular to the plane of the disc with respect to which we evaluate the orbital elements, the nodal precession with respect to the plane of the e -structure transforms to extreme oscillations of inclination over the whole interval $\langle 0, \pi \rangle$ with respect to the plane of the disc (see Sect. 2.3.3 for details). Averaging of eccentricity and inclination over an increasing number of such oscillating orbits then leads to the accelerated increase of their root-mean-square values observed in Fig. 2.4 (phases ‘II’ and ‘III’). The rate of this increase is determined by the radial density profile of the disc.

The existence of two different phases of the accelerated evolution of the root-mean-square eccentricity and inclination of the orbits in the disc can be understood from Fig. 2.8 which shows the evolution of eccentricity e and inclination i of two orbits from the innermost parts of the disc. We see that, for both orbits, the oscillations of inclination do not immediately cover the whole interval $\langle 0; \pi \rangle$ but only a small fraction of it (hereafter ‘basic’ mode). Furthermore, the full amplitude of the oscillations of inclination (hereafter ‘extreme’ mode) is reached at different times for each of the two orbits ($t \approx 5 \times 10^3 T_{\text{orb}}(R_{\text{in}})$ and $t \approx 3 \times 10^3 T_{\text{orb}}(R_{\text{in}})$ in the top and bottom panel, respectively). Eccentricity of the orbits oscillates to very high values already in the basic mode. However, in the extreme mode, the orbits spend notably longer periods of time in their high-eccentricity states. This behaviour is typical for most of the orbits from the affected parts of the disc. We thus suggest that the first phase of the accelerated evolution of the root-mean-square eccentricity and inclination observed in Fig. 2.4 (phase ‘II’) corresponds to the averaging over the oscillations in the basic mode. When most of the orbits in the affected parts of the disc are already oscillating in the basic mode, the root-mean-square eccentricity and inclination saturate, further showing slower increase due to averaging over an increasing number of orbits that start to oscillate in the extreme mode (phase ‘III’).

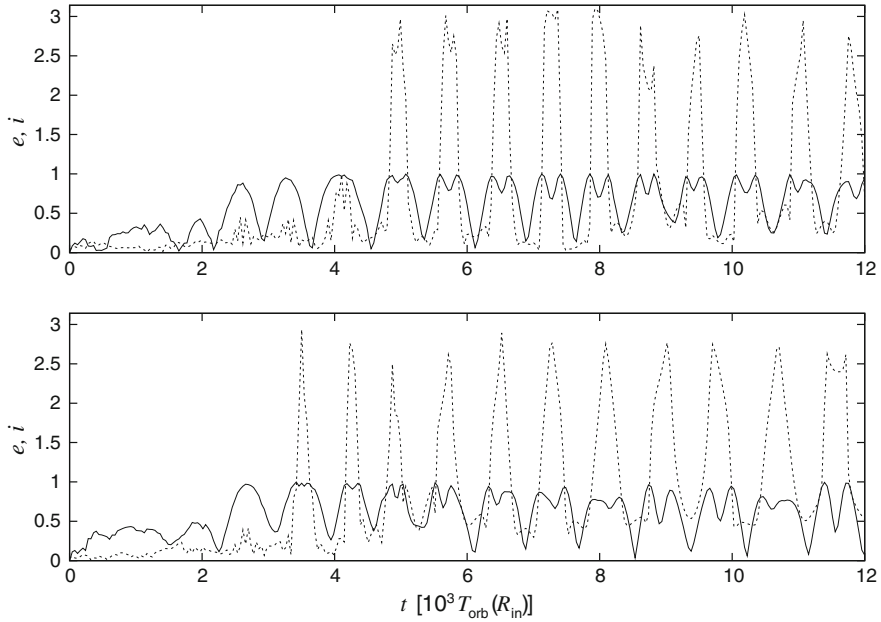


Fig. 2.8 Evolution of the orbital eccentricity e (solid lines) and inclination i (dashed lines) of two typical stars from the innermost parts of the disc within the canonical configuration (see Table 2.1). We observe that both elements undergo extreme oscillations. The maximum value of eccentricity, $e \rightarrow 1$, is reached when the orbits are roughly perpendicular to the parent disc: $i \approx \pi/2$. We further see that both orbits start their oscillations (basic mode) at approximately the same time: $t \approx 2 \times 10^3 T_{\text{orb}}(R_{\text{in}})$. It also turns out that, for each of the orbits, the oscillations of inclination reach the extreme amplitude $(0; \pi)$ at different times

2.2.4 e -Instability in the Disc

Similarly, to the case of the cluster in the axisymmetric potential of the disc, our calculations reveal that also the disc under the effect of the flattened potential of the e -structure in the cluster evolves its own e -structure. This finding is demonstrated in Fig. 2.9 which shows the distribution of directions of the eccentricity vectors of the innermost orbits in the disc in terms of angles Ω_e and i_e at $t = 0$ (left panel) and $t \approx 6 \times 10^3 T_{\text{orb}}(R_{\text{in}})$ (right panel). We observe that, in accord with the assumed initial axial symmetry of the disc, the distribution in the left panel is uniform with respect to Ω_e (abscissa). Furthermore, since the disc is assumed to be initially thin, the individual vectors are confined to a narrow belt along the equatorial line of the plot. In the right panel, however, we can see that nearly all of the displayed orbits belong to a single compact group and, therefore, they form a significant e -structure. Despite the similar orientation of the apsidal lines of the orbits in the e -structure, the initial overall axial symmetry of the mass distribution in the disc does not appear

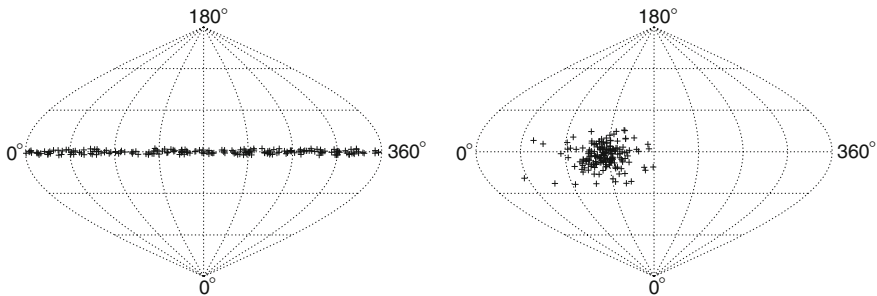
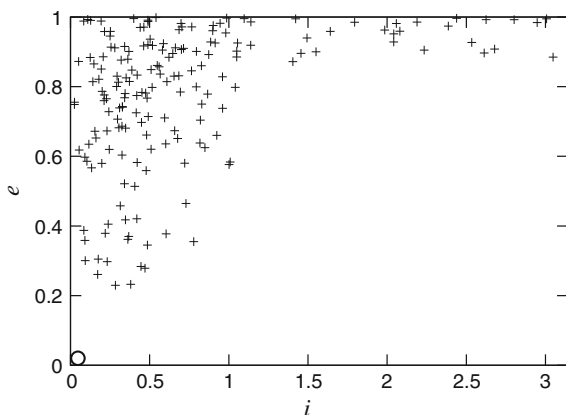


Fig. 2.9 Directions of the eccentricity vectors of the orbits from the disc with the osculating semi-major axis $a < 1.5 R_{\text{in}}$ in terms of angles Ω_e (abscissa) and i_e (ordinate) in sinusoidal projection. The initial state is displayed in the *left panel* while the *right panel* describes the directions at $t \approx 6 \times 10^3 T_{\text{orb}}(R_{\text{in}})$. We see that, in the evolved state, nearly all of the displayed orbits belong to a single compact group, thus forming a significant *e*-structure. Model parameters are set to their canonical values (see Table 2.1)

Fig. 2.10 Eccentricity e and inclination i of the innermost orbits in the evolved disc ($t \approx 6 \times 10^3 T_{\text{orb}}(R_{\text{in}})$; only orbits with the osculating semi-major axis $a < 1.5 R_{\text{in}}$ are displayed). We see that the orbits are mostly low-inclined and highly eccentric. The initial state is denoted by the *empty circle*. Model parameters are set to their canonical values (see Table 2.1)



to be disturbed dramatically by the *e*-structure formation (see the panels in the left column of Fig. 2.11), similar to the case of the *e*-structure in the cluster.

Our results further show that this *e*-structure is, unlike the *e*-structure in the cluster, formed by rather eccentric and mostly low-inclined orbits (see Fig. 2.10). On the other hand, similar to the *e*-structure in the cluster, the *e*-structure in the disc also rotates around the initial symmetry axis of the disc. Furthermore, we find that the individual orbits from the *e*-structure in the disc rotate much more synchronously in comparison with the orbits from the *e*-structure in the cluster. In other words, the rotation of the *e*-structure in the disc much more resembles the rotation of a solid body (see Fig. 2.11). We attribute this finding to the fact that the stellar density in the initially thin disc is higher than in the spherical cluster. Consequently, the *e*-structure in the disc represents a deeper potential well that bounds the individual orbits more

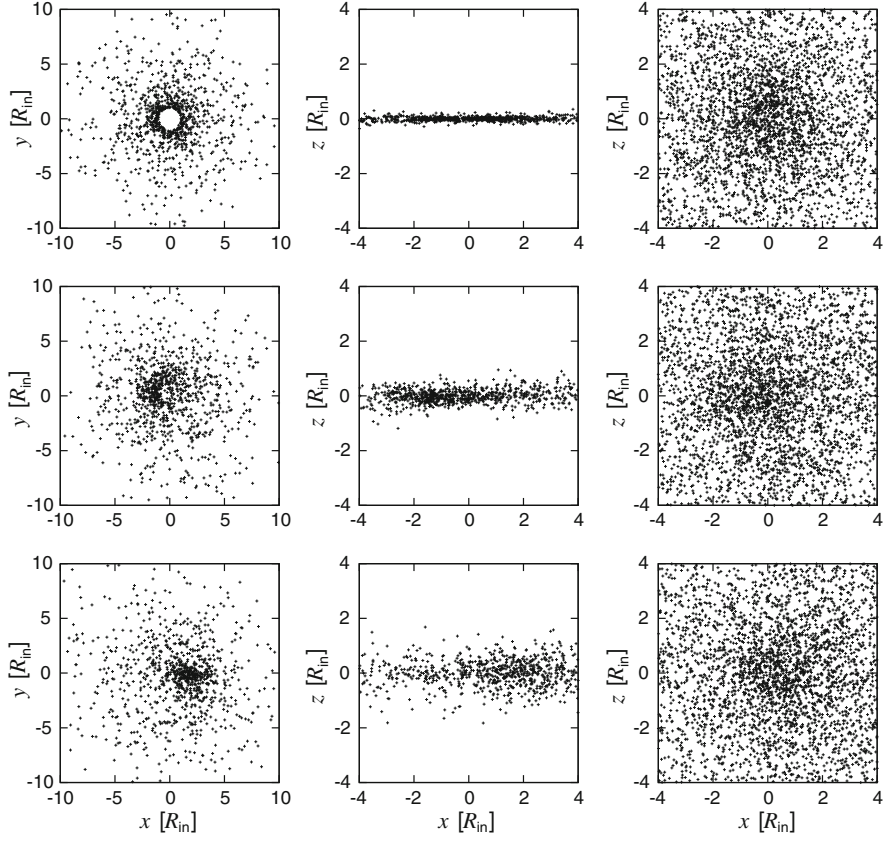


Fig. 2.11 The positions of the stars in the disc (left and middle column) and the cluster (right column) in projection onto the xy -plane (left column) and the xz -plane (middle and right column; zoomed on the central parts of the disc and the cluster) at three different times: $t = 0$ (top panels), $t \approx 2.8 \times 10^3 T_{\text{orb}}(R_{\text{in}})$ (middle panels; corresponds to the time when the e -structures in the cluster and the disc reach similar orientation) and $t \approx 10.9 \times 10^3 T_{\text{orb}}(R_{\text{in}})$ (bottom panels). Model parameters are set to their canonical values (see Table 2.1)

strongly than in the case of the e -structure in the cluster. This appears to be crucial for the mutual interaction of these two e -structures.

2.2.5 Interaction of the e -Structures in the Cluster and the Disc

We have learned that both the cluster and the disc form, during their orbital evolution, significant e -structures slowly rotate around the symmetry axis of the disc. It further turns out that the rate of this rotation is different for the two e -structures, which

leads to a continuous change of their relative orientation and, eventually, to a state in which the typical eccentricity vectors in the two e -structures point in roughly the same direction.

Furthermore, we have also seen that the e -structures cause the Kozai-Lidov oscillations of eccentricity and inclination of the individual orbits. Since these oscillations occur on a timescale that is shorter than the timescale of the rotation of the e -structures (thus even shorter in comparison with the timescale of the change of the relative orientation of the e -structures), the individual orbits certainly undergo a full Kozai-Lidov cycle during the period of time in which the orientations of the e -structures are similar. As we have mentioned above, the e -structure in the disc appears to be self-bound more strongly in comparison with the e -structure in the cluster. Hence, once the orbits from the e -structure in the cluster incline, during their Kozai-Lidov cycles, to the plane of the disc, they become dynamically coupled with the e -structure in the disc, precessing further synchronously with this e -structure.

Due to this mechanism, the innermost e -structure in the cluster is entirely absorbed by the e -structure in the disc as soon as they reach similar orientations. Consequently, the innermost parts of the investigated stellar system further contain only one coherently rotating e -structure that includes nearly all of the stars from this region. Moreover, eccentricity and inclination of some of the orbits from the cluster even start to oscillate in a way typical for the orbits from the disc (cf. Figs. 2.5, $t \gtrsim 3.5 \times 10^3 T_{\text{orb}}(R_{\text{in}})$, and 2.8, $t \gtrsim 5 \times 10^3 T_{\text{orb}}(R_{\text{in}})$). Such orbits from the cluster thus effectively become part of the disc. As we can see in the right column of Fig. 2.11, however, this effect does not lead to any significant flattening of the cluster in the direction perpendicular to the plane of the disc.

Let us also mention that the plots in the right column of Fig. 2.11 reveal another feature of the cluster evolution. In particular, although the initial spherical symmetry of the core of the cluster is disturbed only slightly during the evolution, in the evolved state, the core is not centred precisely on the SMBH anymore.

2.2.6 Propagation of the e -Instability to Farther Regions

So far, we have been investigating the evolution of the inner parts of the stellar system. However, our calculations show that the e -instability in the cluster propagates also to its outer parts. This effect is demonstrated in Fig. 2.12 which shows the eccentricity vector angle Ω_e of the stars in the cluster, depending on their instantaneous distance from the central SMBH at four different stages of the orbital evolution of the cluster. As we can see in the top-left panel, the initial distribution is in accord with the assumed initial spherical symmetry of the cluster. On the other hand, the remaining three panels show overdensities which propagate outwards in the plot and indicate presence of e -structures even in the outer parts of the cluster.

Furthermore, similar to the innermost region of the cluster, the flattened potential of the disc leads to the Kozai-Lidov oscillations of eccentricity and inclination of the individual orbits in the more distant regions of the cluster as soon as the spherical

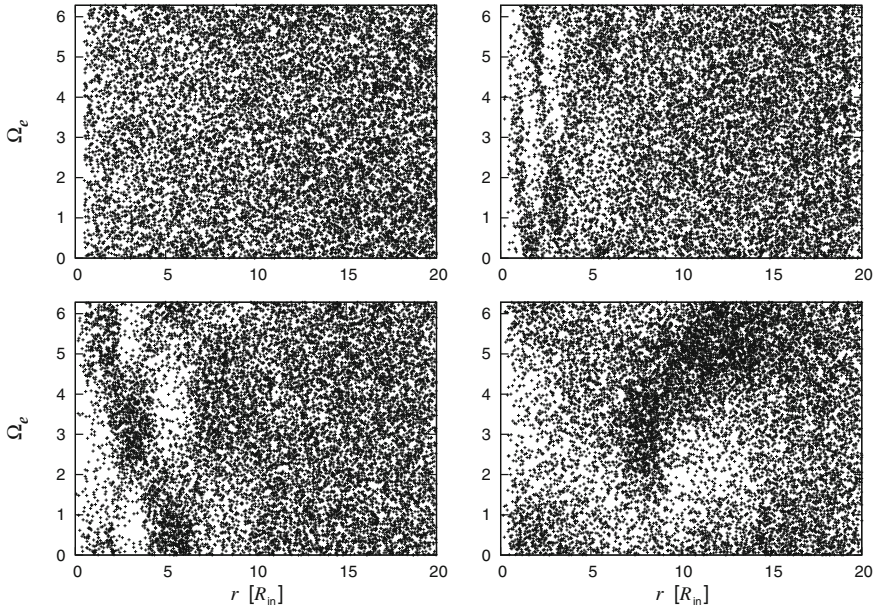


Fig. 2.12 Values of the eccentricity vector angle Ω_e and the instantaneous distance r from the SMBH of the stars in the cluster at four different stages of the cluster evolution: $t = 0$ (*top-left panel*), $t \approx 1.2 \times 10^3 T_{\text{orb}}(R_{\text{in}})$ (*top-right panel*), $t \approx 2.4 \times 10^3 T_{\text{orb}}(R_{\text{in}})$ (*bottom-left panel*) and $t \approx 12 \times 10^3 T_{\text{orb}}(R_{\text{in}})$ (*bottom-right panel*). We see that the e -instability gradually propagates to the outer parts of the cluster. Model parameters are set to their canonical values (see Table 2.1)

symmetry of the mean potential is disturbed by the formation of the e -structures. As the potential of the disc in these regions is weaker, however, the corresponding timescale of the oscillations is longer and, therefore, the eccentricity of the orbits in the outermost e -structures is still quite low (see Fig. 2.13).

Finally, let us mention that, unlike the cluster, the disc forms only one dominating e -structure that includes nearly all of its stars, as can be inferred from Fig. 2.14.

2.3 Basic Processes

In the previous section, we have described the complex evolution of the stellar system that consists of an initially thin disc which is embedded in an extended spherical cluster, both centred on the SMBH, by means of the full N -body modelling. In the following, we investigate the individual basic processes included in this evolution separately, by means of simplified models.

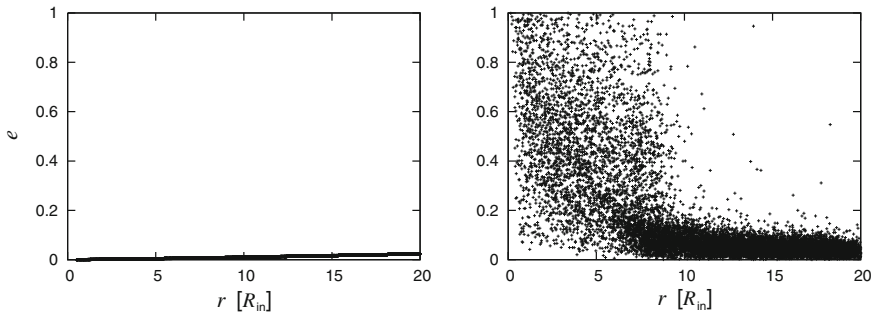


Fig. 2.13 Values of eccentricity e and the instantaneous distance r from the SMBH of the stars in the cluster. The left panel shows the initial state when the orbits are geometrically circular (the Keplerian eccentricity of the orbits in the outer parts of the cluster is thus larger than zero). The right panel describes the state at $t \approx 12 \times 10^3 T_{\text{orb}}(R_{\text{in}})$ (cf. the bottom-right panel of Fig. 2.12). We see that, in the inner parts of the cluster, the orbital eccentricities are increased due to the Kozai-Lidov oscillations in the potential of the disc. Model parameters are set to their canonical values (see Table 2.1)

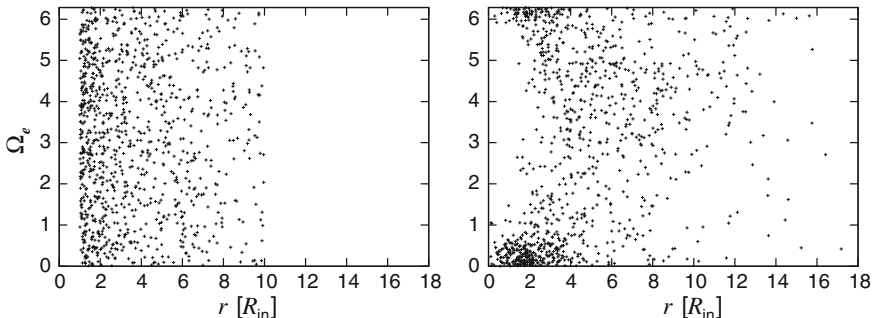


Fig. 2.14 Values of the eccentricity vector angle Ω_e and the instantaneous distance r from the SMBH of all the stars in the disc at $t = 0$ (left panel) and $t \approx 12 \times 10^3 T_{\text{orb}}(R_{\text{in}})$ (right panel). We observe that nearly all of the stars in the disc are concentrated in one large e -structure. Model parameters are set to their canonical values (see Table 2.1)

2.3.1 Kozai-Lidov Dynamics in the Cluster

We first analyse the orbital evolution of an initially spherically symmetric cluster of test particles whose motions around the dominating central SMBH are perturbed by a predefined distant infinitesimally thin ring (hereafter K0a-model; see Table 2.1). In other words, we study the statistical effects of the Kozai-Lidov dynamics of the individual stars from the cluster in the potential of the ring. For this purpose, we follow the orbital evolution of the cluster numerically, by means of the N -body integration code Mbody (Šubr 2006) which is more suitable for this particular setting. The use of an independent numerical integrator also enables us to test our results for systematic flaws that might have been introduced by specific numerical methods implemented

in the NBODY6 code used in the case of the canonical configuration. The effect of test particles is reached by decreasing the mass of the individual stars from the cluster to an extremely low value, $m_c \sim 10^{-12} M_\bullet$.

Depending on the initial conditions of the individual orbits from the cluster, the corresponding Kozai-Lidov diagrams may be of two qualitatively different topologies (see Fig. 1.2): (i) solely rotational diagrams, or (ii) diagrams with the librational and the outer rotational region. In the later case, the diagrams contain the separatrix contour which resembles a straight radial line near the point of its intersection at $e = 0$. Along the isocontours in the vicinity of these parts of the separatrix, the orbital argument of pericentre thus remains roughly constant (in both the librational and the outer rotational region). As the cluster is assumed to be initially spherically symmetric, the distribution of $\cos i$ of the stellar orbits is uniform. Furthermore, within the K0a-model, we consider the orbits to be initially near-circular and, therefore, also the initial distribution of the Kozai integral of motion (1.11) in the cluster is uniform. Since the value of the Kozai integral that corresponds to the Kozai limit is $c_1 = \sqrt{3/5} \approx 0.8$, we see that the Kozai-Lidov diagrams for most of the orbits in the cluster contain both the librational and outer rotational region. As a result, the Kozai-Lidov cycles for the majority of the orbits in the cluster include the phase with nearly constant argument of pericentre. This indicates that, during the evolution of the cluster of test particles, an overabundance of orbits with a specific value of ω might appear.

Given the diagrams with both the librational and the outer rotational regions, the Kozai-Lidov Eq. (1.32) imply that a stellar orbit with initial argument of pericentre $\omega_0 \approx 0$ or π has $(d\omega/dt)_0 > 0$. We thus understand that the evolutionary tracks of all the orbits in the outer rotational region follow the isocontours of the diagram in the counter-clockwise direction. Similarly, as we can deduce for initial $\omega_0 \approx \pi/2$ or $3\pi/2$, the same direction is followed for all the orbits that belong to either of the librational lobes. Since the initially near-circular orbits form a compact group in the centre of the diagram, the overabundant values of ω should, in the first phase of the evolution, correspond to the straight part of the separatrix in the first and the third quadrant, i.e. $\omega_{\text{const}} \approx 1$ and ≈ 4 , respectively (see the middle panels of Fig. 2.15). Subsequently, as the orbits in the cluster shift in the diagram due to their evolution, the surroundings of the other two branches of the separatrix in the second and the fourth quadrant of the diagram become populated as well and, therefore, another two overabundances at $\omega_{\text{const}} \approx 2$ and ≈ 5 appear (bottom panels of Fig. 2.15).

Figure 2.16 demonstrates the non-uniform distribution of the orbital arguments of pericentre in the cluster in terms of the eccentricity vector angles Ω_e (abscissa) and i_e (ordinate). In particular, the right panel displays the state that corresponds to the bottom panels of Fig. 2.15, i.e. the state in which all four overabundances are already evolved. For geometrical reasons, the orbits with $\omega \approx 1$ and ≈ 2 have the same value of $i_e \approx 60^\circ$, forming the lower horizontal belt in the right panel of Fig. 2.16. The orbits with $\omega \approx 4$ and ≈ 5 then form the upper belt.

Given the same initial conditions for the cluster, the results would be somewhat different if the distant thin ring were replaced by a disc-like perturbation. As we have mentioned in Sect. 1.3, in such a case, the Kozai-Lidov diagrams may, for

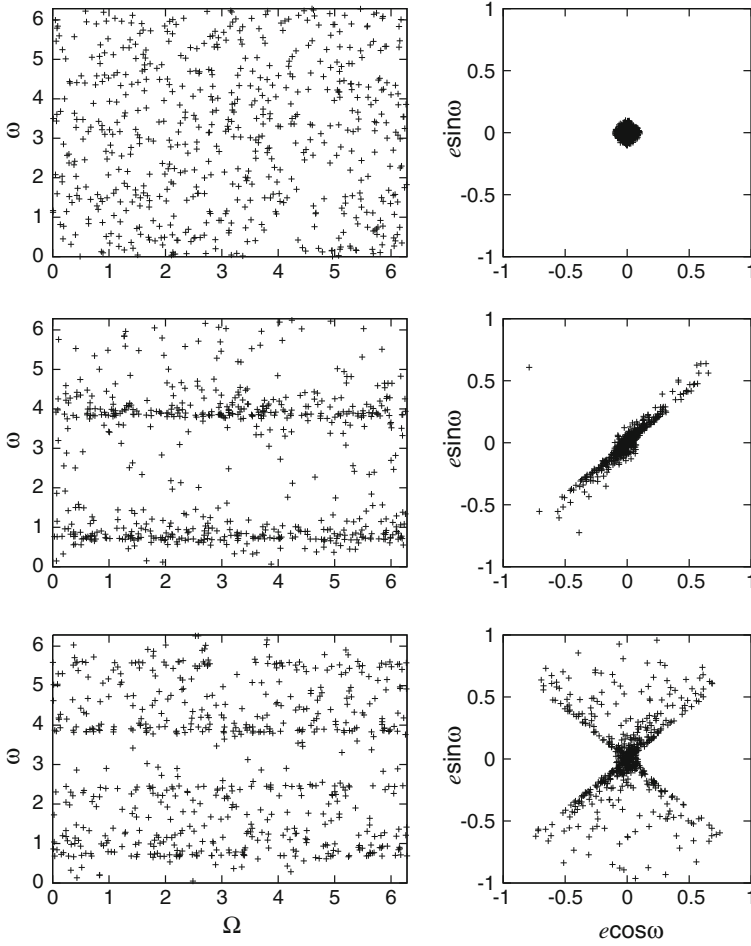


Fig. 2.15 Formation of the overabundances of specific values of the orbital argument of pericentre ω in the cluster of test particles under the perturbative gravitational influence of the distant thin ring (K0a-model; see Table 2.1). The *left panels* demonstrate the evolution of the distribution of argument of pericentre ω and longitude of the ascending node Ω of all the orbits in the cluster. The *right panels* show the position of the orbits in the Kozai-Lidov diagrams. In the initial state (*top panels*), the distribution of both ω and Ω is uniform and all the orbits are found near the origin, $e = 0$, of the diagram. In the evolved state displayed in the *middle panels* ($t \approx 2.4 \times 10^3 T_{\text{orb}}(R_{\text{in}})$), we see the overabundances of $\omega \approx 1$ and ≈ 4 which correspond to the branches of the separatrix contour in the first and the third quadrant of the diagram, respectively. At a later stage of the evolution ($t \approx 5.6 \times 10^3 T_{\text{orb}}(R_{\text{in}})$; *bottom panels*), also the overabundances of $\omega \approx 2$ and ≈ 5 are visible. The distribution of the nodal longitude Ω is uniform in all states, which is in accord with the axial symmetry of the problem

low enough values of the Kozai integral (1.11), contain the inner rotational region around the origin $e = 0$. Hence, the initially near-circular orbits that have such

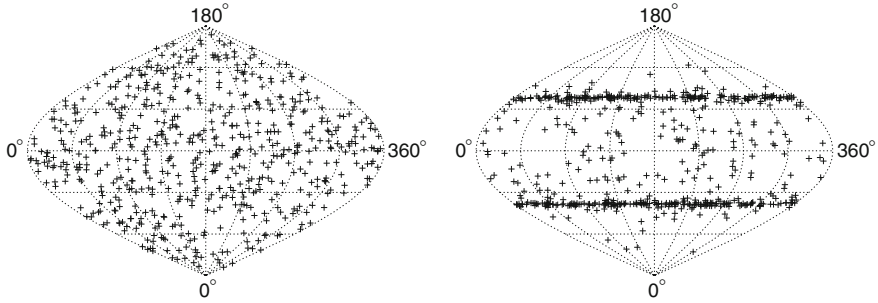


Fig. 2.16 Directions of the eccentricity vectors of all the orbits in the cluster of test particles in terms of angles Ω_e (abscissa) and i_e (ordinate) in sinusoidal projection. The initial distribution (*left panel*) is in accord with the assumed initial spherical symmetry of the cluster. In the evolved state ($t \approx 5.6 \times 10^3 T_{\text{orb}}(R_{\text{in}})$; *right panel*), we see two horizontal belts (cf. the *bottom panels* of Fig. 2.15 and the *right panel* of Fig. 2.6). The model parameters are set to values that correspond to the K0a-model (see Table 2.1)

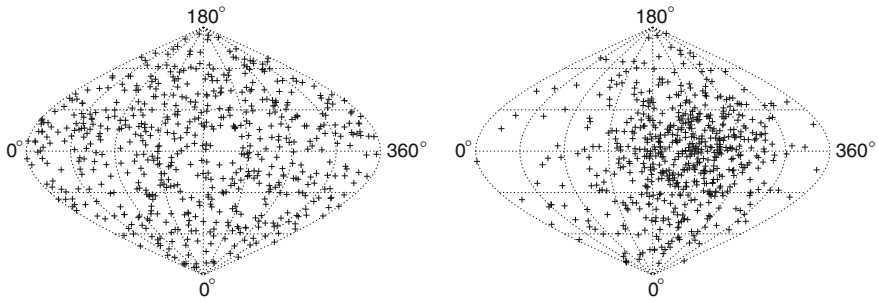


Fig. 2.17 Directions of the eccentricity vectors of all the orbits in the self-gravitating cluster in terms of angles Ω_e (abscissa) and i_e (ordinate) in sinusoidal projection. The initial distribution (*left panel*) is in accord with the assumed initial spherical symmetry of the cluster. In the evolved state ($t \approx 2.4 \times 10^3 T_{\text{orb}}(R_{\text{in}})$; *right panel*), nearly all of the orbits belong to a single e -structure. Model parameters correspond to the K0b-model (see Table 2.1)

values of c cannot reach the critical location in the diagram as they are confined to the inner rotational region. Such orbits thus do not contribute to formation of the overabundances. Consequently, the significance of these features is lower as they are generated by a lower number of orbits with moderate values of c .

Overabundances similar to those described above have also been observed for the cluster in the canonical configuration (see the right panel of Fig. 2.6). In the context of this section, we thus argue that they result from the Kozai-Lidov dynamics of the stars from the cluster in the potential of the disc, forming just after the damping effect of the spherical mean potential of the cluster is sufficiently disturbed by the ongoing formation of the cluster e -structure. On the other hand, the formation of the e -structure gradually decreases the significance of the overabundances and, eventually, the overabundances are entirely absorbed by the e -structure.

2.3.2 Formation of the *e*-Structure in the Cluster

Within the K0a-model, we have investigated the orbital evolution of the initially spherically symmetric star cluster under the assumption that the masses of its individual stars are negligibly small. Here, we consider the stars to have a non-negligible mass, $m_c \sim 10^{-5} M_\bullet$. In doing so, we include their mutual gravitational interaction (hereafter the K0b-model; see Table 2.1).

The results of our calculations within the K0b-model are demonstrated in Fig. 2.17 which displays the initial (left panel) and evolved (right panel) distribution of the eccentricity vector angles Ω_e (abscissa) and i_e (ordinate) of the orbits in the cluster. We see that, while the initial distribution corresponds to the initial spherical symmetry of the cluster, in the evolved state, the orbits form a significant *e*-structure. It thus appears that the *e*-instability is a generic process which occurs in star clusters that are exposed to an axisymmetric perturbation, even if the perturbative potential is predefined (see also Sect. 2.3.4).

Our calculations further show that the orbital properties of this *e*-structure are similar to those of the *e*-structure observed in the canonical configuration. In particular, the *e*-structure slowly rotates around the symmetry axis of the disc and, at the time of its formation, it consists of mostly low-eccentric orbits whose inclinations are distributed similar to the initial state of the cluster, showing the mean value of $\approx \pi/2$ (see Fig. 2.18). Like in the case of the canonical configuration, we attribute this to the damping effect of the mean potential of the cluster ($N_c m_c = 0.15 M_\bullet$) which suppresses the Kozai-Lidov mechanism in the potential of the ring, as long as its spherical symmetry is not disturbed by the formation of the *e*-structure.

2.3.3 Kozai-Lidov Dynamics in the Disc

Within the canonical configuration, the *e*-structures in the evolved cluster form a rather complex system (see Sect. 2.2.6). In order to describe their impact on the embedded disc, we attempt to simplify the problem by neglecting the gravity of all but the innermost *e*-structure. This approximation is well justified by the following argument. The *e*-structures in the cluster affect the disc on the Kozai-Lidov timescale $T_{\text{KL}} \propto R_{\text{estr}}^3 / M_{\text{estr}}$, where M_{estr} and R_{estr} denote the mass and the characteristic radius of the *e*-structure, respectively. Since the initial radial density profile of the cluster is, in the canonical configuration, given by (1.30), the mass of the *e*-structure can be estimated as $M_{\text{estr}} \propto R_{\text{estr}}^{1/4}$. Consequently, we find that the Kozai-Lidov timescale grows steeply as $T_{\text{KL}} \propto R_{\text{estr}}^{11/4}$. Due to the assumed surface density profile of the disc, $\Sigma(R) \propto R^{-2}$, majority of the stars in the disc are located in its inner parts, i.e. in the immediate vicinity of the innermost *e*-structure in the cluster. Hence, it appears that the innermost *e*-structure represents the dominating perturbation of the stellar motions in the disc since the Kozai-Lidov timescale for this *e*-structure is much shorter than those of the *e*-structures at larger radii.

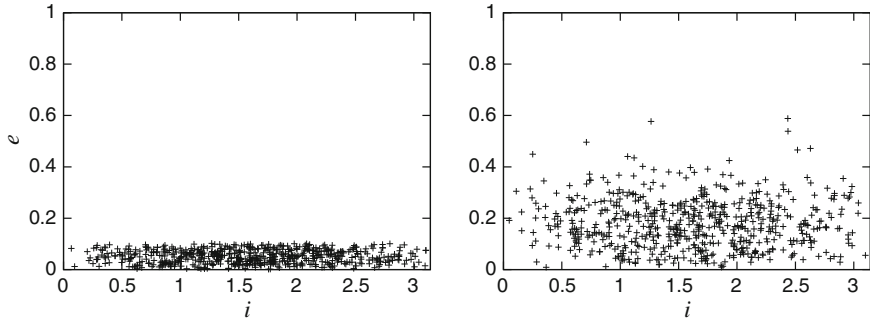


Fig. 2.18 Eccentricity e and inclination i of all the orbits in the cluster in its initial state (*left panel*) and shortly after the formation of a significant e -structure ($t \approx 2.4 \times 10^3 T_{\text{orb}}(R_{\text{in}})$; *right panel*; see also Fig. 2.17). We observe that the orbits in the e -structure are still rather low-eccentric with inclinations close to their initial values. Model parameters correspond to the K0b-model (see Table 2.1)

Furthermore, as the rotation of the e -structures around the symmetry axis of the disc is slow (see Sect. 2.2.2), we neglect this feature and approximate the e -structure by a static predefined potential, in particular, by the potential of an infinitesimally thin ring that is centred on the SMBH and perpendicular to the plane of the disc. For simplicity, we also exclude the residual spherically symmetric component of the potential of the cluster. Moreover, we consider the stars in the disc to be test particles, thus neglecting their mutual gravitational interaction.

In summary, we focus on the model with the following three components (hereafter K1a-model, see Table 2.1):

- the central SMBH represented by the Keplerian potential,
- the stellar disc formed by test particles,
- the innermost e -structure in the cluster modelled by the predefined potential of an infinitesimally thin ring which is perpendicular to the plane of the disc.

The orbital evolution of the disc within the K1a-model is followed numerically, by means of the Mbody code. The xy -plane of our Cartesian reference frame is defined as the plane of symmetry of the disc. The direction of the z -axis is determined by the initial mean angular momentum of the orbits in the disc, i.e. the stellar motions in the disc are considered to be initially prograde.

As we have learned in Sect. 1.3, the potential of the ring causes the Kozai-Lidov oscillations of eccentricity and inclination with the combined nodal and apsidal precession of the orbits in the disc. Provided the reference plane is identified with the plane of the ring, the orbital elements (e' , i' , Ω' , ω') follow Eqs. (1.12). An example of such an evolution is displayed in Fig. 1.3. However, since we evaluate the orbital elements in the reference plane which is identified with the plane of the disc and, therefore, perpendicular to the ring, the evolution of the elements that describe the spatial orientation of the orbits (i , Ω , ω) is different. On the other hand, evolution of e remains untouched as this element does not depend upon the coordinate system.

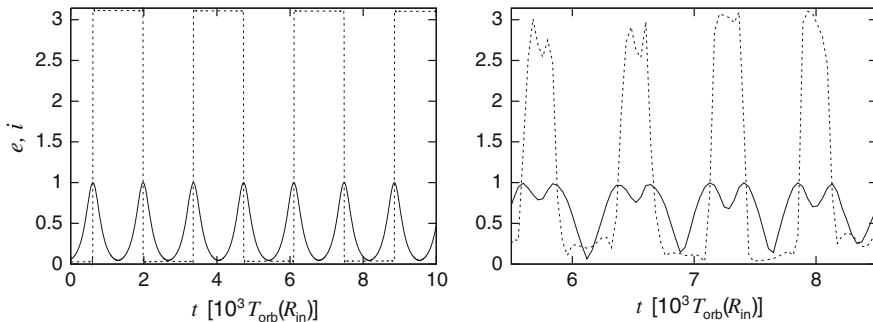


Fig. 2.19 Evolution of eccentricity e (solid lines) and inclination i (dashed lines) of individual stellar orbits from the disc within the K1a-model (*left panel*) and the canonical configuration (*right panel*; cut from the evolution displayed in the bottom panel of Fig. 2.8). We see that both orbits undergo extreme oscillations during which the maximum eccentricity, $e \rightarrow 1$, is reached for $i \approx \pi/2$. Model parameters are summarized in Table 2.1

The left panel of Fig. 2.19 shows the evolution of eccentricity e (solid line) and inclination i (dashed line) of a stellar orbit from the disc within the K1a-model. For the sake of clarity, the chosen orbit is initially almost exactly perpendicular to the plane of the ring: $i'_0 \rightarrow \pi/2$. In such a case, the evolution of i' and Ω' leads to rectangular-shaped oscillations of inclination i over the interval $(0; \pi)$. For orbits that are initially less inclined with respect to the ring, the oscillations of i show periodic variations of their amplitude. Unlike inclination, we see that eccentricity e of the orbit evolves in the same way as we observed in Fig. 1.3. Let us also mention that the maximum of eccentricity, $e \rightarrow 1$, is reached whenever the orbit becomes perpendicular to the parent disc, $i = \pi/2$, in contrary to what we can see in Fig. 1.3.

Evolution of the root-mean-square eccentricity, e_{rms} , and inclination, i_{rms} , of all the orbits in the disc within the K1a-model is displayed in the top panels of Fig. 2.20. We observe that the evolution of both elements consists of three qualitatively different stages: (i) the initial steady phase, (ii) the rapid increase and (iii) the saturated phase of damped oscillations. It turns out that this behaviour is a straightforward consequence of the averaging over a number of individual orbits that undergo the above-described oscillations. In particular, within the K1a-model, the disc is considered to be initially thin and near-circular. Hence, both eccentricities and inclinations of the individual orbits are initially low. As demonstrated in the left panel of Fig. 2.19, the orbits start their evolution in the phase when both $de/dt \approx 0$ and $di/dt \approx 0$. Consequently, also the root-mean-square values of the two elements are, in the initial stage of their evolution, roughly constant. In the case of eccentricity, however, this phase is very short (the rapid increase starts at about $t \approx 10^2 T_{\text{orb}}(R_{\text{in}})$; top-left panel of Fig. 2.20) as the minima of its oscillations are sharp. On the other hand, the initial steady phase of the evolution of the root-mean-square inclination is, due to the rectangular-shaped oscillations, notably longer (until $t \approx 4 \times 10^2 T_{\text{orb}}(R_{\text{in}})$; top-right panel of Fig. 2.20).

Subsequently, as the eccentricity and inclination of the individual orbits in the disc start to oscillate, the root-mean-square values of both elements increase. The rate of

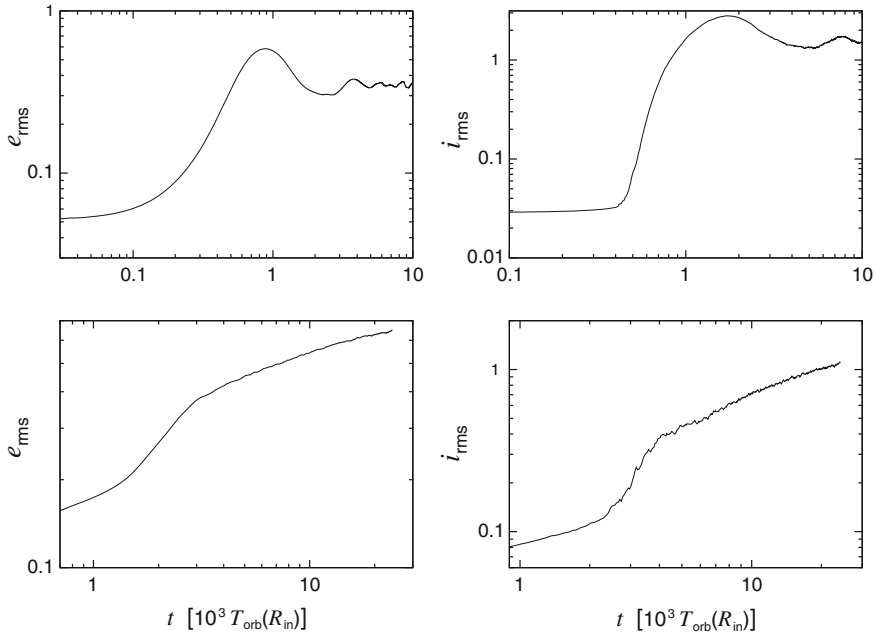


Fig. 2.20 Evolution of the root-mean-square eccentricity e_{rms} (left panels) and inclination i_{rms} (right panels) of the orbits in the disc within the K1a-model (top panels; results averaged over 10 realizations) and the canonical configuration (bottom panels; redrawn from Fig. 2.4; results averaged over 9 realizations). We see that the evolution of both root-mean-square elements within the simple K1a-model includes the accelerated phase, in accord with the results obtained for the canonical configuration. Due to high numerical demands of the problem, we have not been able to reach, in the canonical configuration, the saturated phase of the evolution. Model parameters are summarized in Table 2.1

this increase and the overall shape of the corresponding curve are strongly influenced by the assumed radial density profile of the disc which determines the distribution of the orbital semi-major axes and, consequently, also the periods ($\sim T_{\text{KL}} \propto a^{3/2}$) of the oscillations. In the case of our K1a-model, majority of the orbits are located near the inner edge of the disc, thus having similar semi-major axes. Hence, eccentricity and inclination oscillate with similar frequency for most of the orbits in the disc, which leads to the observed rapid increase of the root-mean-square values of both elements.

Finally, when most of the orbits are oscillating, the root-mean-square values of both elements saturate, further showing only low-amplitude, gradually damped oscillations. The particular shape and amplitude of these oscillations are determined by the radial density profile of the disc. Hence, within the K1a-model, the similar semi-major axes of the orbits in the disc lead to the first smooth bump on the corresponding curves. Later on, as the phases of the oscillations of the individual orbits in the disc disperse, the oscillations of the root-mean-square elements slowly diminish, leaving them roughly constant.

In the context of these findings, we suggest that the accelerated evolution of the root-mean-square eccentricity and inclination of the orbits in the disc observed in the canonical configuration (redrawn in the bottom panels of Fig. 2.20) is, indeed, caused by averaging over an increasing number of oscillating orbits in the flattened potential of the innermost e -structure in the cluster. This conclusion is supported by comparison of the evolution of the typical orbits from the central parts of the disc in the canonical configuration and the K1a-model which is shown in Fig. 2.19. We see that both orbits undergo similar oscillations of their eccentricity and inclination. In particular, the oscillations have nearly the same amplitude and fulfil the condition that $e \rightarrow 1$ for $i \approx \pi/2$. On the other hand, when the orbit from the canonical disc reaches the retrograde inclination $i \approx \pi$, its eccentricity does not decrease to zero, unlike the orbit from the K1a-model. Similarly, the curves that describe the evolution of the root-mean-square elements in the two configurations are also somewhat different (see Fig. 2.20). We attribute these differences to the approximations introduced in the K1a-model. Most notably, the innermost e -structure in the cluster in the canonical configuration is not geometrically thin and it is developed gradually, in contrast to the predefined thin ring considered in the K1a-model. Furthermore, while the stars in the canonical configuration are gravitating, in the K1a-model, they are treated as test particles.

2.3.4 Formation of the e -Structure in the Disc

The top panels of Fig. 2.21 display the comparison of the initial (left panel) and evolved distribution (right panel) of the eccentricity vector angles Ω_e and i_e of the orbits in the disc within the K1a-model. As we can see, the initial distribution is in agreement with the assumption that the disc is initially thin and axially symmetric. In the evolved state, however, we observe that the individual eccentricity vectors are concentrated in four roughly equally populated compact groups which are uniformly distributed along the equatorial line of the plot with the step of $\Delta\Omega_e \approx \pi/2$. Furthermore, we find that these groups are not rotating in any direction. On the other hand, they show a continuous exchange of the individual orbits that freely migrate among them (see the outliers in the top-right panel of Fig. 2.21).

The picture changes if the disc is considered to be self-gravitating, i.e. if the mutual gravitational interaction of the individual stars in the disc is included (hereafter K1b-model, see Table 2.1). In particular, as we observe in the bottom-left panel of Fig. 2.21, the four groups are replaced by a single e -structure that includes most of the orbits from the disc. Our calculations further show that this e -structure slowly rotates around the initial symmetry axis of the disc and consists of mostly eccentric and low-inclined orbits (see the left panel of Fig. 2.22).

A similar e -structure developed in the disc within the canonical configuration (see the bottom-right panel of Fig. 2.21 and the right panel of Fig. 2.22). Hence, based on the results presented in this section, we suggest that the e -instability in the disc in the canonical configuration is, indeed, due to the flattened potential of the innermost

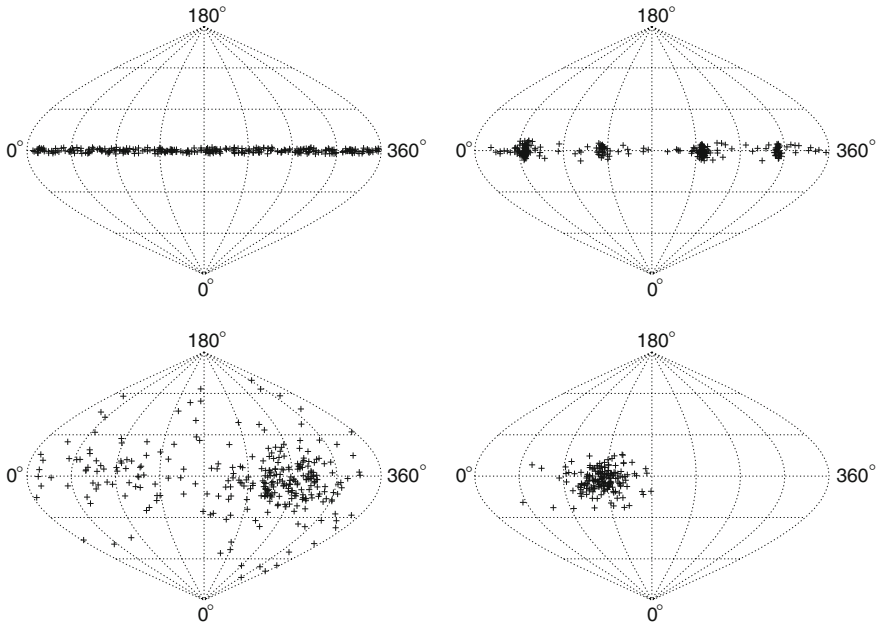


Fig. 2.21 Directions of the eccentricity vectors of the orbits in the disc in terms of angles Ω_e (abscissa) and i_e (ordinate): the initial state (*top-left panel*; all orbits in the disc are displayed) and the evolved state within the K1a-model ($t \approx 3 \times 10^3 T_{\text{orb}}(R_{\text{in}})$; *top-right panel*; all orbits displayed), the evolved state within the K1b-model ($t \approx 10 \times 10^3 T_{\text{orb}}(R_{\text{in}})$; *bottom-left panel*; all orbits displayed) and the evolved state in the canonical configuration ($t \approx 6 \times 10^3 T_{\text{orb}}(R_{\text{in}})$; *bottom-right panel*, redrawn from Fig. 2.9; only orbits with the osculating semi-major axes $a < 1.5 R_{\text{in}}$ are shown). We see that the self-gravitating disc in the predefined potential of thin ring (K1b-model) forms a significant e -structure, similar to the disc in the canonical configuration. Model parameters are summarized in Table 2.1

e -structure in the cluster. Let us note that the e -structure in the disc appears to be formed, in both configurations, with a roughly perpendicular orientation ($\Delta\Omega_e \approx \pi/2$) to the plane of symmetry of the perturbing potential: the infinitesimally thin ring in the case of the K1b-model and the innermost e -structure in the cluster in the canonical configuration.

2.4 Discussion of Model Parameters

In the canonical configuration, we have treated the spherical cluster as a group of $N_c = 1.25 \times 10^4$ gravitating particles. In order to investigate the impact of the number of particles in the cluster upon the acquired results, we have performed two additional sets of calculations with $N_c = 5 \times 10^4$ and 6.25×10^3 (see also Table 2.1, models A and D, respectively). The total mass of the cluster in these models is

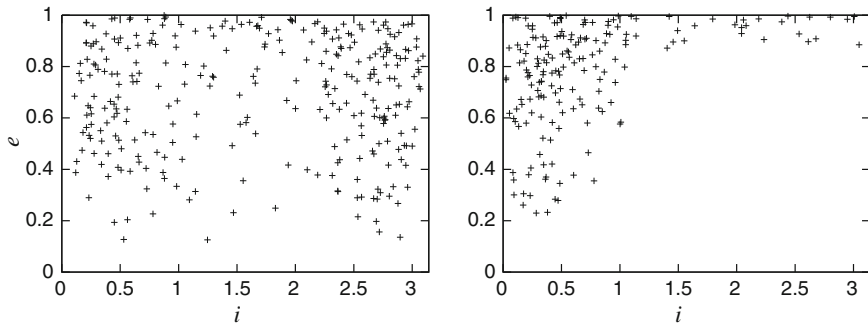


Fig. 2.22 Eccentricity e and inclination i of all the orbits in the evolved disc within the K1b-model (*left panel*) and of the innermost orbits (with the osculating semi-major axes $a < 1.5 R_{\text{in}}$) from the disc in the canonical configuration (*right panel*; redrawn from Fig. 2.10). We see that the orbits are mostly low-inclined and highly eccentric in both cases. Model parameters are summarized in Table 2.1

equal to the canonical one, i.e. the masses of the individual particles are smaller (larger). Evolution of the root-mean-square eccentricity, e_{rms} , and inclination, i_{rms} , in comparison to the canonical configuration is shown in the top panels of Fig. 2.23. We see that the corresponding curves are nearly identical in all three cases. This indicates that, while the treatment of the cluster gravity affects the evolution of the disc significantly (analytic potential vs. particles), the concrete number of particles in the cluster is of no importance.

On the other hand, when the total mass of the cluster is assumed to be ten times larger than the canonical one (see Table 2.1, model H), our calculations show that the accelerated evolution of both root-mean-square elements onsets by a factor of 3–4 sooner and also the rate of the growth is noticeably higher (bottom panels of Fig. 2.23, dashed lines). We attribute these results to higher masses of the e -structures that form in the cluster which, therefore, cause a faster evolution of the orbits in the disc.

The solid lines in the bottom panels of Fig. 2.23 describe the case when we have included, beside the same spherical cluster of particles as within model D, an additional predefined analytic spherically symmetric potential (see Table 2.1, model M). Its radial profile and strength parameter have been considered to correspond to the matter distribution in the cluster within model D. We observe that none of the root-mean-square elements undergoes the accelerated phase of its evolution, which is likely to be due to the damping effect of the predefined analytic spherical potential that suppresses the Kozai-Lidov mechanism in the potential of the e -structures in the cluster. On the other hand, our results indicate that the e -structure formation neither in the cluster nor in the disc is affected significantly by the additional potential, except for the fact that both e -structures appear to be formed with the same initial orientation (see Fig. 2.24).

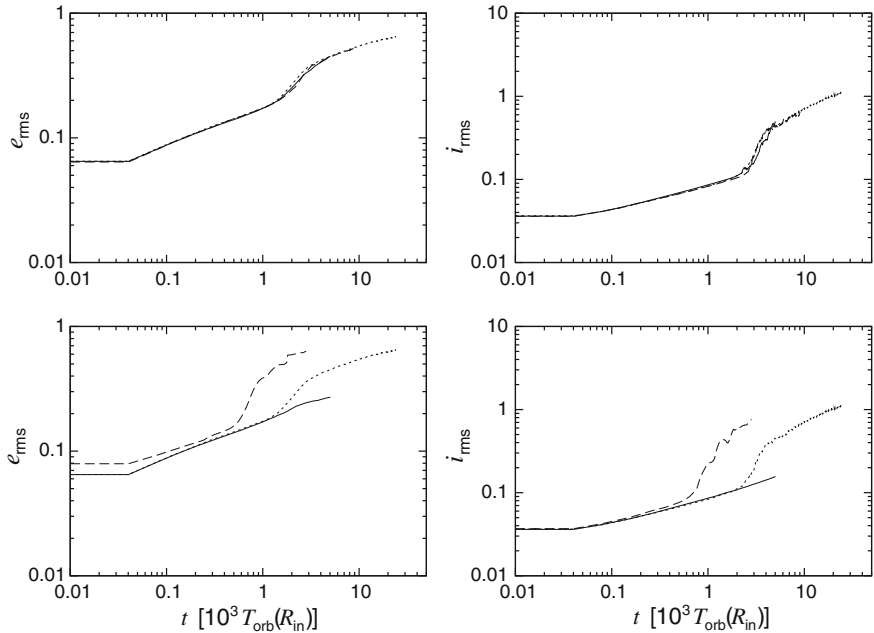


Fig. 2.23 Evolution of the root-mean-square eccentricity e_{rms} (left panels) and inclination i_{rms} (right panels) of the orbits in the disc in various configurations in comparison to the results acquired in the canonical configuration (depicted by the dotted lines; redrawn from Fig. 2.4; results averaged over 9 realizations). The top panels demonstrate the effect of the number of particles, N_c , in the cluster whose total mass is kept unchanged: $N_c = 5 \times 10^4$ (dashed lines; model A; results are averaged over 5 realizations) and 6.25×10^3 (solid lines; model D; results are averaged over 7 realizations). The bottom panels show the results obtained in two cases: with the total mass of particles in the cluster, $N_c m_c$, ten times larger than the canonical one (dashed lines; model H; results averaged over 9 realizations) and with an additional predefined analytic spherically symmetric potential (solid lines; model M; results averaged over 11 realizations). Model parameters are summarized in Table 2.1

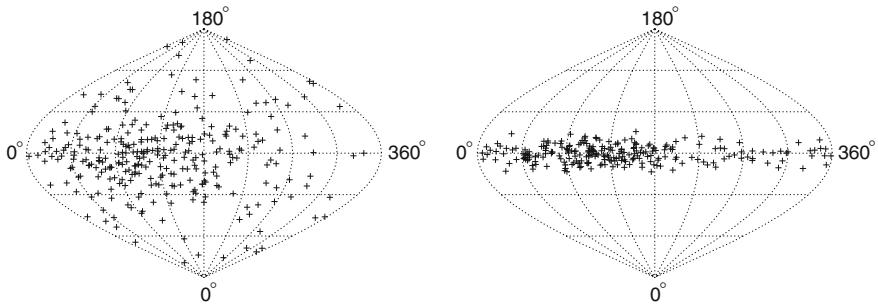


Fig. 2.24 Distribution of the directions of the eccentricity vectors of the orbits in the cluster (left panel) and the disc (right panel) at $t \approx 3.2 \times 10^3 T_{\text{orb}}(R_{\text{in}})$ within model M (only orbits with the osculating semi-major axes $a < 2 R_{\text{in}}$ are displayed). We see that both the cluster and the disc evolve significant e -structures. Model parameters are summarized in Table 2.1

References

- Aarseth S. J., 2003, *Gravitational N-Body Simulations*. Cambridge Univ. Press, Cambridge
- Bartko H. et al., 2009, *ApJ*, 697, 1741
- Bartko H. et al., 2010, *ApJ*, 708, 834
- Bender R. et al., 2005, *ApJ*, 631, 280
- Haas J., Šubr L., 2012, *JPhCS*, 372, 012059
- Lauer T. R., Bender R., Kormendy J., Rosenfield P., Green R. F., 2012, *ApJ*, 745, 121
- Levin Y., Beloborodov A. M., 2003, *ApJ*, 590, L33
- Paumard T. et al., 2006, *ApJ*, 643, 1011
- Šubr L., 2006, private communication



<http://www.springer.com/978-3-319-03649-6>

Symmetries and Dynamics of Star Clusters

Haas, J.

2014, XVI, 79 p. 42 illus., Hardcover

ISBN: 978-3-319-03649-6